

## Accelerated Article Preview

# SARS-CoV-2 infection induces long-lived bone marrow plasma cells in humans

---

Received: 20 December 2020

---

Accepted: 14 May 2021

---

Accelerated Article Preview Published  
online 24 May 2021

---

Cite this article as: Turner, J. S. et al.  
SARS-CoV-2 infection induces long-lived  
bone marrow plasma cells in humans.  
*Nature* <https://doi.org/10.1038/s41586-021-03647-4> (2021).

---

Jackson S. Turner, Wooseob Kim, Elizaveta Kalaidina, Charles W. Goss, Adriana M. Rauseo,  
Aaron J. Schmitz, Lena Hansen, Alem Haile, Michael K. Klebert, Iskra Pusic,  
Jane A. O'Halloran, Rachel M. Presti & Ali H. Ellebedy

---

This is a PDF file of a peer-reviewed paper that has been accepted for publication. Although unedited, the content has been subjected to preliminary formatting. Nature is providing this early version of the typeset paper as a service to our authors and readers. The text and figures will undergo copyediting and a proof review before the paper is published in its final form. Please note that during the production process errors may be discovered which could affect the content, and all legal disclaimers apply.

# SARS-CoV-2 infection induces long-lived bone marrow plasma cells in humans

<https://doi.org/10.1038/s41586-021-03647-4>

Received: 20 December 2020

Accepted: 14 May 2021

Published online: 24 May 2021

Jackson S. Turner<sup>1</sup>, Wooseob Kim<sup>1</sup>, Elizaveta Kalaidina<sup>2</sup>, Charles W. Goss<sup>3</sup>, Adriana M. Rauseo<sup>4</sup>, Aaron J. Schmitz<sup>1</sup>, Lena Hansen<sup>1,5</sup>, Alem Haile<sup>6</sup>, Michael K. Klebert<sup>6</sup>, Iskra Pusic<sup>7</sup>, Jane A. O'Halloran<sup>4</sup>, Rachel M. Presti<sup>4,9</sup> & Ali H. Ellebedy<sup>1,8,9✉</sup>

Long-lived bone marrow plasma cells (BMPCs) are a persistent and essential source of protective antibodies<sup>1–7</sup>. Severe acute respiratory syndrome coronavirus 2 (SARS-CoV-2) convalescent individuals have a significantly lower risk of reinfection<sup>8–10</sup>. Nonetheless, it has been reported that anti-SARS-CoV-2 serum antibodies experience rapid decay in the first few months after infection, raising concerns that long-lived BMPCs may not be generated and humoral immunity against this virus may be short-lived<sup>11–13</sup>. Here we demonstrate that in patients who experienced mild infections (n=77), serum anti-SARS-CoV-2 spike (S) antibodies decline rapidly in the first 4 months after infection and then more gradually over the following 7 months, remaining detectable at least 11 months after infection. Anti-S antibody titers correlated with the frequency of S-specific BMPCs obtained from bone marrow aspirates of 18 SARS-CoV-2 convalescent patients 7 to 8 months after infection. S-specific BMPCs were not detected in aspirates from 11 healthy subjects with no history of SARS-CoV-2 infection. We demonstrate that S-binding BMPCs are quiescent, indicating that they are part of a long-lived compartment. Consistently, circulating resting memory B cells directed against the S protein were detected in the convalescent individuals. Overall, we show that SARS-CoV-2 infection induces a robust antigen-specific, long-lived humoral immune response in humans.

Reinfections by seasonal coronaviruses occur 6–12 months after the previous infection, indicating that protective immunity against these viruses may be short-lived<sup>14,15</sup>. Early reports documenting rapidly declining antibody titers in convalescent SARS-CoV-2 patients in the first several months after infection suggested that protective immunity against SARS-CoV-2 may be similarly transient<sup>11–13</sup>. It was also suggested that SARS-CoV-2 infection may fail to elicit a functional germinal center response, which would interfere with the generation of long-lived plasma cells<sup>3–5,7,16</sup>. Later reports analyzing samples collected approximately 4 to 6 months after infection indicate that SARS-CoV-2 antibody titers decline more slowly<sup>8,17–21</sup>. Durable serum antibody titers are maintained by long-lived plasma cells, non-replicating, antigen-specific plasma cells that are detected in bone marrow long after the disappearance of the antigen<sup>1–7</sup>. We sought to determine whether they were detectable in SARS-CoV-2 convalescent patients approximately 7 months after infection.

## Biphasic decay of anti-S antibody titers

Blood samples were collected approximately 1 month after onset of symptoms from seventy-seven SARS-CoV-2 convalescent volunteers

(49% female, 51% male, median age 49), the majority of whom had experienced mild illness (7.8% hospitalized, Extended Data Tables 1 and 2). Follow-up blood samples were collected three times at approximately 3-month intervals. Twelve convalescent participants received either the BNT162b2 or the mRNA-1273 SARS-CoV-2 vaccine between the last two timepoints; these post-vaccination samples were not included in our analyses. Additionally, bone marrow aspirates were collected from eighteen of the participants 7 to 8 months after infection and from eleven healthy volunteers with no history of SARS-CoV-2 infection or vaccination. Follow-up bone marrow aspirates were collected from five of the eighteen and one additional convalescent donor approximately 11 months after infection. (Fig. 1a, Extended Data Tables 3 and 4). We first performed a longitudinal analysis of circulating anti-SARS-CoV-2 serum antibodies. While anti-SARS-CoV-2 spike (S) IgG antibodies were undetectable in blood from controls, 74 of 77 convalescent participants had detectable serum titers approximately 1 month after onset of symptoms. Between 1- and 4-months post symptom onset, overall anti-S IgG titers decreased from a mean of 6.3 to 5.7 (mean difference 0.59±0.06,  $P<0.001$ ). However, in the interval between 4- and 11-months post symptom onset, the decay rate slowed, and mean titers declined from 5.7 to 5.3 (mean difference 0.44±0.10,  $P<0.001$ , Fig. 1a).

<sup>1</sup>Department of Pathology and Immunology, Washington University School of Medicine, St. Louis, MO, USA. <sup>2</sup>Division of Allergy and Immunology, Department of Internal Medicine, Washington University School of Medicine, St. Louis, MO, USA. <sup>3</sup>Division of Biostatistics, Washington University School of Medicine, St. Louis, MO, USA. <sup>4</sup>Division of Infectious Diseases, Department of Internal Medicine, Washington University School of Medicine, St. Louis, MO, USA. <sup>5</sup>Influenza Centre, Department of Clinical Science, University of Bergen, 5021, Bergen, Norway. <sup>6</sup>Clinical Trials Unit, Washington University School of Medicine, St. Louis, MO, USA. <sup>7</sup>Division of Oncology, Department of Internal Medicine, Washington University School of Medicine, St. Louis, MO, USA. <sup>8</sup>The Andrew M. and Jane M. Bursky Center for Human Immunology & Immunotherapy Programs, Washington University School of Medicine, Saint Louis, MO, USA. <sup>9</sup>Center for Vaccines and Immunity to Microbial Pathogens, Washington University School of Medicine, Saint Louis, MO, USA. ✉e-mail: ellebedy@wustl.edu

In contrast to the anti-S antibody titers, IgG titers against the 2019/2020 inactivated seasonal influenza virus vaccine were detected in all control and SARS-CoV-2 convalescent participants and declined much more gradually, if at all over the course of the study, with mean titers decreasing from 8.0 to 7.9 (mean difference  $0.16 \pm 0.06$ ,  $P=0.042$ ) and 7.9 to 7.8 (mean difference  $0.02 \pm 0.08$ ,  $P=0.997$ ) across the 1-to-4- and 4-to-11-month intervals post symptom onset, respectively (Fig. 1b).

### Induction of S-binding long-lived BMPCs

The relatively rapid early decline in anti-S IgG followed by slower decay is consistent with a transition of serum antibodies from being secreted by short-lived plasmablasts to a smaller but more persistent population of long-lived plasma cells generated later in the immune response. The majority of this latter population resides in bone marrow<sup>1-6</sup>. To investigate whether SARS-CoV-2 convalescent patients developed a virus specific long-lived BMPC compartment, we examined their bone marrow aspirates obtained approximately 7 and 11 months after infection for anti-SARS-CoV-2 S-specific BMPCs. We magnetically enriched BMPCs from the aspirates and then quantified the frequencies of those secreting IgG and IgA directed against the 2019/2020 influenza virus vaccine, tetanus/diphtheria vaccine, and SARS-CoV-2 S protein by ELISpot (Fig. 2a). Frequencies of influenza and tetanus/diphtheria vaccine specific BMPCs were comparable between control and convalescent participants. IgG- and IgA-secreting S-specific BMPCs were detected in 15 and 9 of the 19 convalescent participants, respectively, but not in any of the 11 control participants (Fig. 2b). Importantly, none of the convalescent patients had detectable S-specific antibody secreting cells in blood at the time of bone marrow sampling, indicating that the detected BMPCs represent bone marrow-resident cells and not contamination from circulating plasmablasts. Frequencies of anti-S IgG BMPCs were stable among the five participants sampled a second time approximately 4m later, and anti-S IgA BMPC frequencies were stable in four of the five, with one decreasing below the limit of detection (Fig. 2c). Consistent with their stable BMPC frequencies, anti-S IgG titers in the five participants remained consistent between 7- and 11-months post symptom onset. IgG titers measured against the receptor binding domain (RBD) of S, a primary target of neutralizing antibodies, were detected in four of the five convalescent patients and were also stable between 7- and 11-months post symptom onset (Fig. 2d). Frequencies of anti-S IgG BMPCs showed a modest but significant correlation with circulating anti-S IgG titers 7-8 months post symptom onset in convalescent participants, consistent with long-term maintenance of antibody levels by these cells. In accordance with previous reports<sup>22-24</sup>, frequencies of influenza vaccine-specific IgG BMPCs and antibody titers exhibited a strong and significant correlation (Fig. 2e). Nine of the aspirates from controls and twelve of the eighteen collected 7m post symptom onset yielded a sufficient number of BMPCs for additional analysis by flow cytometry. We stained these samples intracellularly with fluorescently labeled S and influenza virus hemagglutinin (HA) probes to identify and characterize antigen specific BMPCs. As controls, we also intracellularly stained PBMC from healthy volunteers 1 week after SARS-CoV-2 or seasonal influenza virus vaccination (Fig. 3a, Extended Data Fig. 1a-c). Consistent with the ELISpot data, low frequencies of S-binding BMPCs were detected in ten of the twelve convalescent specimens analyzed, but not in any of the nine control specimens (Fig. 3b). While both recently generated circulating plasmablasts and S- and HA-binding BMPCs expressed Blimp1, BMPCs were differentiated by the lack of expression of Ki-67, indicating a quiescent state, as well as higher levels of CD38 (Fig. 3c).

### Robust S-binding memory B cell response

Memory B cells (MBCs) form the second arm of humoral immune memory. Upon antigen re-exposure, MBCs rapidly expand and differentiate

into antibody-secreting plasmablasts. We examined the frequency of SARS-CoV-2 specific circulating MBCs in convalescent patients as well as in the healthy controls. We stained peripheral blood mononuclear cells with fluorescently labeled S probes and determined the frequency of S-binding MBCs among isotype-switched IgD<sup>lo</sup> CD20<sup>+</sup> MBCs by flow cytometry. For comparison, we co-stained the cells with fluorescently labeled influenza virus hemagglutinin (HA) probes (Fig. 4a). S-binding MBCs were identified in convalescent patients in the first sample collected approximately 1 month after onset of symptoms, with comparable frequencies to influenza HA-binding memory B cells (Fig. 4b). S-binding memory B cells were maintained for at least 7m post symptom onset and were present at significantly higher frequencies compared to healthy controls, comparable to frequencies of influenza HA-binding memory B cells identified in both groups (Fig. 4c).

### Discussion

This study sought to determine whether SARS-CoV-2 infection induces antigen-specific long-lived BMPCs in humans. We detected SARS-CoV-2 S-specific BMPCs in aspirates from 15 of 19 convalescent patients, and in none from the 11 control participants. Frequencies of anti-S IgG BMPCs modestly correlated with serum IgG titers 7-8 months after infection. Phenotypic analysis by flow cytometry demonstrated that S-binding BMPCs were quiescent, and their frequencies were largely consistent in five paired aspirates collected 7- and 11-months post symptom onset. Importantly, we detected no S-binding cells among plasmablasts in blood samples collected at the same time as the bone marrow aspirates by ELISpot or flow cytometry in any of the convalescent or control samples. Altogether, these data indicate mild SARS-CoV-2 infection elicits a long-lived BMPC response. Additionally, we showed that S-binding MBCs in blood of convalescent patients are present at similar frequencies to those directed against influenza virus HA. Overall, our results are consistent with SARS-CoV-2 infection eliciting a canonical T-dependent B cell response, in which an early transient burst of extrafollicular plasmablasts generates a wave of serum antibodies that decline relatively quickly. This is followed by more stably maintained serum antibody levels that are supported by long-lived BMPCs.

While this overall trend captures the serum antibody dynamics of the majority of participants, we observed that in three participants, anti-S serum antibody titers increased between 4- and 7-months post symptom onset after having initially declined between 1 and 4 months. This could be stochastic noise, could represent increased net binding affinity as early plasmablast-derived antibodies are replaced by those from affinity-matured BMPCs, or could represent increases in antibody concentration from reencounter with the virus (although none of the participants in our cohort tested positive a second time). While anti-S IgG titers in the convalescent cohort were relatively stable in the interval between 4- and 11-months post symptom onset, they did measurably decrease, in contrast to anti-influenza virus vaccine titers. While this could represent an intrinsically less durable anti-S BMPC response compared to that against influenza virus, the largely stable frequencies of anti-S BMPCs measured in the same individuals 7- and 11-months post symptom onset argue against this possibility. It is possible that the decline reflects a final waning of early plasmablast-derived antibodies. It is also possible that the lack of decline in influenza titers was due to boosting through exposure to influenza antigens from infection or vaccination. Our data suggest that SARS-CoV-2 infection induces a germinal center response in humans because long-lived BMPCs are thought to be predominantly germinal center-derived<sup>7</sup>. This is consistent with a report demonstrating increased levels of somatic hypermutation in MBCs targeting the receptor binding domain of the S protein in SARS-CoV-2 convalescent patients at 6 months compared to 1 month after infection<sup>20</sup>.

To our knowledge, the current study provides the first direct evidence for induction of antigen specific BMPCs after a viral infection in humans.

However, we do acknowledge several limitations. Although we detected anti-S IgG antibodies in serum at least 7 months after infection in all 19 of the convalescent donors from whom we obtained bone marrow aspirates, we failed to detect S-specific BMPCs in four donors. Serum anti-S antibody titers in those four donors were low, suggesting that S-specific BMPCs may potentially be present at very low frequencies that are below our limit of detection. Another limitation is that we do not know the fraction of the S-binding BMPCs detected in our study that encodes neutralizing antibodies. SARS-CoV-2 S protein is the main target of neutralizing antibodies<sup>17,25–30</sup> and correlation between serum anti-S IgG binding and neutralization titers has been documented<sup>17,31</sup>. Further studies will be required to determine the epitopes targeted by BMPCs and MBCs as well as their clonal relatedness. Finally, while our data document a robust induction of long-lived BMPCs after SARS-CoV-2 infection, it is critical to note that our convalescent patients mostly experienced mild infections. Our data are consistent with a report showing that individuals who recovered rapidly from symptomatic SARS-CoV-2 infection generated a robust humoral immune response<sup>32</sup>. Therefore, it is possible that more severe SARS-CoV-2 infections could lead to a different outcome with respect to long-lived BMPC frequencies due to dysregulated humoral immune responses. This, however, has not been the case in survivors of the 2014 West African Ebola virus outbreak in whom severe viral infection induced long-lasting antigen-specific serum IgG antibodies<sup>33</sup>.

Long-lived BMPCs provide the host with a persistent source of preformed protective antibodies and are therefore needed to maintain durable immune protection. However, longevity of serum anti-S IgG antibodies is not the only determinant of how durable immune-mediated protection will be. Indeed, isotype-switched MBCs can rapidly differentiate into antibody secreting cells upon pathogen reexposure, offering a second line of defense<sup>34</sup>. Encouragingly, the frequency of S-binding circulating MBCs 7 months after infection was similar compared to those directed against contemporary influenza HA antigens. Overall, our data provide strong evidence that SARS-CoV-2 infection in humans robustly establishes the two arms of humoral immune memory: long-lived BMPC and MBCs. These findings provide an immunogenicity benchmark for SARS-CoV-2 vaccines and a foundation for assessing the durability of primary humoral immune responses induced after viral infections in humans.

## Online content

Any methods, additional references, Nature Research reporting summaries, source data, extended data, supplementary information, acknowledgements, peer review information; details of author contributions and competing interests; and statements of data and code availability are available at <https://doi.org/10.1038/s41586-021-03647-4>.

1. Benner, R., Meima, F., van der Meulen, G. M. & van Muiswinkel, W. B. Antibody formation in mouse bone marrow. I. Evidence for the development of plaque-forming cells in situ. *Immunology* **26**, 247–255 (1974).
2. Manz, R. A., Thiel, A. & Radbruch, A. Lifetime of plasma cells in the bone marrow. *Nature* **388**, 133–134 (1997).
3. Slifka, M. K., Antia, R., Whitmire, J. K. & Ahmed, R. Humoral Immunity Due to Long-Lived Plasma Cells. *Immunity* **8**, 363–372 (1998).
4. Hammarlund, E. et al. Duration of antiviral immunity after smallpox vaccination. *Nat. Med.* **9**, 1131–1137 (2003).

5. Halliley, J. L. et al. Long-Lived Plasma Cells Are Contained within the CD19–CD38hiCD138+ Subset in Human Bone Marrow. *Immunity* **43**, 132–145 (2015).
6. Mei, H. E. et al. A unique population of IgG-expressing plasma cells lacking CD19 is enriched in human bone marrow. *Blood* **125**, 1739–1748 (2015).
7. Nutt, S. L., Hodgkin, P. D., Tarlinton, D. M. & Corcoran, L. M. The generation of antibody-secreting plasma cells. *Nat. Rev. Immunol.* **15**, 160–171 (2015).
8. Hall, V. J. et al. SARS-CoV-2 infection rates of antibody-positive compared with antibody-negative health-care workers in England: a large, multicentre, prospective cohort study (SIREN). *The Lancet* S0140673621006759 (2021) [https://doi.org/10.1016/S0140-6736\(21\)00675-9](https://doi.org/10.1016/S0140-6736(21)00675-9).
9. Houlihan, C. F. et al. Pandemic peak SARS-CoV-2 infection and seroconversion rates in London frontline health-care workers. *The Lancet* **396**, e6–e7 (2020).
10. Lumley, S. F. et al. Antibodies to SARS-CoV-2 are associated with protection against reinfection. <http://medrxiv.org/lookup/doi/10.1101/2020.11.18.20234369> (2020) <https://doi.org/10.1101/2020.11.18.20234369>.
11. Long, Q.-X. et al. Clinical and immunological assessment of asymptomatic SARS-CoV-2 infections. *Nat. Med.* **26**, 1200–1204 (2020).
12. Ibarondo, F. J. et al. Rapid Decay of Anti-SARS-CoV-2 Antibodies in Persons with Mild Covid-19. *N. Engl. J. Med.* **383**, 1085–1087 (2020).
13. Seow, J. et al. Longitudinal observation and decline of neutralizing antibody responses in the three months following SARS-CoV-2 infection in humans. *Nat. Microbiol.* **5**, 1598–1607 (2020).
14. Edridge, A. W. D. et al. Seasonal coronavirus protective immunity is short-lasting. *Nat. Med.* **26**, 1691–1693 (2020).
15. Callow, K. A., Parry, H. F., Sergeant, M. & Tyrrell, D. A. The time course of the immune response to experimental coronavirus infection of man. *Epidemiol. Infect.* **105**, 435–446 (1990).
16. Kaneko, N. et al. Loss of Bcl-6-Expressing T Follicular Helper Cells and Germinal Centers in COVID-19. *Cell* **183**, 143–157.e13 (2020).
17. Wajnberg, A. et al. Robust neutralizing antibodies to SARS-CoV-2 infection persist for months. *Science* eabd7728 (2020) <https://doi.org/10.1126/science.abd7728>.
18. Isho, B. et al. Persistence of serum and saliva antibody responses to SARS-CoV-2 spike antigens in COVID-19 patients. *Sci. Immunol.* **5**, (2020).
19. Dan, J. M. et al. Immunological memory to SARS-CoV-2 assessed for greater than six months after infection. *bioRxiv* 2020.11.15.383323 (2020) <https://doi.org/10.1101/2020.11.15.383323>.
20. Gaebler, C. et al. Evolution of Antibody Immunity to SARS-CoV-2. <http://biorxiv.org/lookup/doi/10.1101/2020.11.03.367391> (2020) <https://doi.org/10.1101/2020.11.03.367391>.
21. Rodda, L. B. et al. Functional SARS-CoV-2-Specific Immune Memory Persists after Mild COVID-19. *Cell* (2020) <https://doi.org/10.1016/j.cell.2020.11.029>.
22. Davis, C. W. et al. Influenza vaccine-induced human bone marrow plasma cells decline within a year after vaccination. *Science* **370**, 237–241 (2020).
23. Tureson, I. Distribution of Immunoglobulin-containing Cells in Human Bone Marrow and Lymphoid Tissues. *Acta Med. Scand.* **199**, 293–304 (2009).
24. Pritz, T. et al. Plasma cell numbers decrease in bone marrow of old patients. *Eur. J. Immunol.* **45**, 738–746 (2014).
25. Shi, R. et al. A human neutralizing antibody targets the receptor binding site of SARS-CoV-2. *Nature* **584**, 120–124 (2020).
26. Cao, Y. et al. Potent Neutralizing Antibodies against SARS-CoV-2 Identified by High-Throughput Single-Cell Sequencing of Convalescent Patients' B Cells. *Cell* **182**, 73–84.e16 (2020).
27. Robbiani, D. F. et al. Convergent antibody responses to SARS-CoV-2 in convalescent individuals. *Nature* **584**, 437–442 (2020).
28. Kreer, C. et al. Longitudinal Isolation of Potent Near-Germline SARS-CoV-2-Neutralizing Antibodies from COVID-19 Patients. *Cell* **182**, 843–854.e12 (2020).
29. Alsoussi, W. B. et al. A Potently Neutralizing Antibody Protects Mice against SARS-CoV-2 Infection. *J. Immunol.* **205**, 915–922 (2020).
30. Wang, C. et al. A human monoclonal antibody blocking SARS-CoV-2 infection. *Nat. Commun.* **11**, 2251 (2020).
31. Wang, K. et al. Longitudinal Dynamics of the Neutralizing Antibody Response to Severe Acute Respiratory Syndrome Coronavirus 2 (SARS-CoV-2) Infection. *Clin. Infect. Dis.* ciaa1143 (2020) <https://doi.org/10.1093/cid/ciaa1143>.
32. Chen, Y. et al. Quick COVID-19 Healers Sustain Anti-SARS-CoV-2 Antibody Production. *Cell* S0092867420314586 (2020) <https://doi.org/10.1016/j.cell.2020.10.051>.
33. Davis, C. W. et al. Longitudinal Analysis of the Human B Cell Response to Ebola Virus Infection. *Cell* **177**, 1566–1582.e17 (2019).
34. Ellebedy, A. H. et al. Defining antigen-specific plasmablast and memory B cell subsets in human blood after viral infection or vaccination. *Nat. Immunol.* **17**, 1226–1234 (2016).

**Publisher's note** Springer Nature remains neutral with regard to jurisdictional claims in published maps and institutional affiliations.

© The Author(s), under exclusive licence to Springer Nature Limited 2021

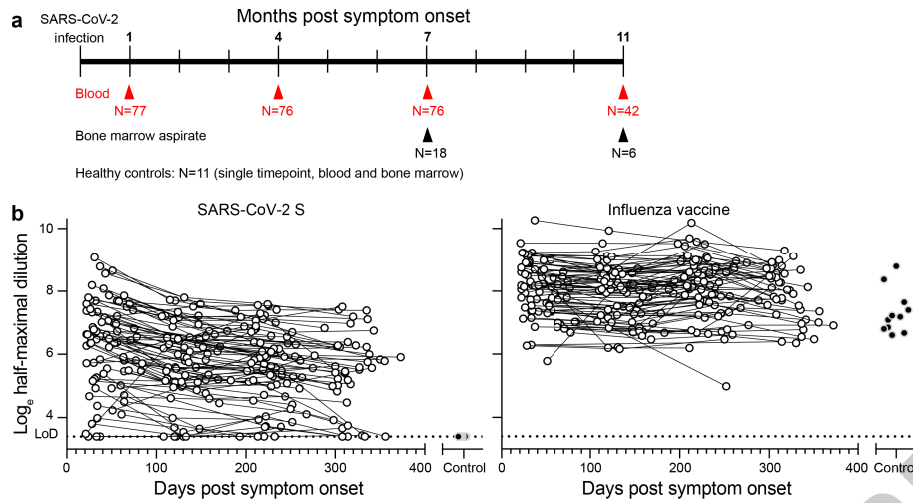


**Fig. 1 | SARS-CoV-2 infection elicits durable serum anti-spike antibody titers. a**, Study design. Seventy-seven SARS-CoV-2 convalescent patients with mild disease (ages 21–69) were enrolled and blood was collected approximately 1 month, 4 months, 7 months, and 11 months post onset of symptoms. Bone marrow aspirates were collected from eighteen of the participants 7 to 8 months after infection and from eleven healthy volunteers (ages 23–60) with no history of SARS-CoV-2 infection. Follow-up bone marrow aspirates were

collected from five of the eighteen convalescent donors and one additional donor approximately 11 months after infection. **b**, Blood IgG titers against S (left) and influenza virus vaccine (right) measured by ELISA in convalescent patients (white circles) at the indicated time post onset of symptoms and controls (black circles). Dotted line indicates limit of detection. Means and pairwise differences at each timepoint were estimated using a linear mixed model analysis.

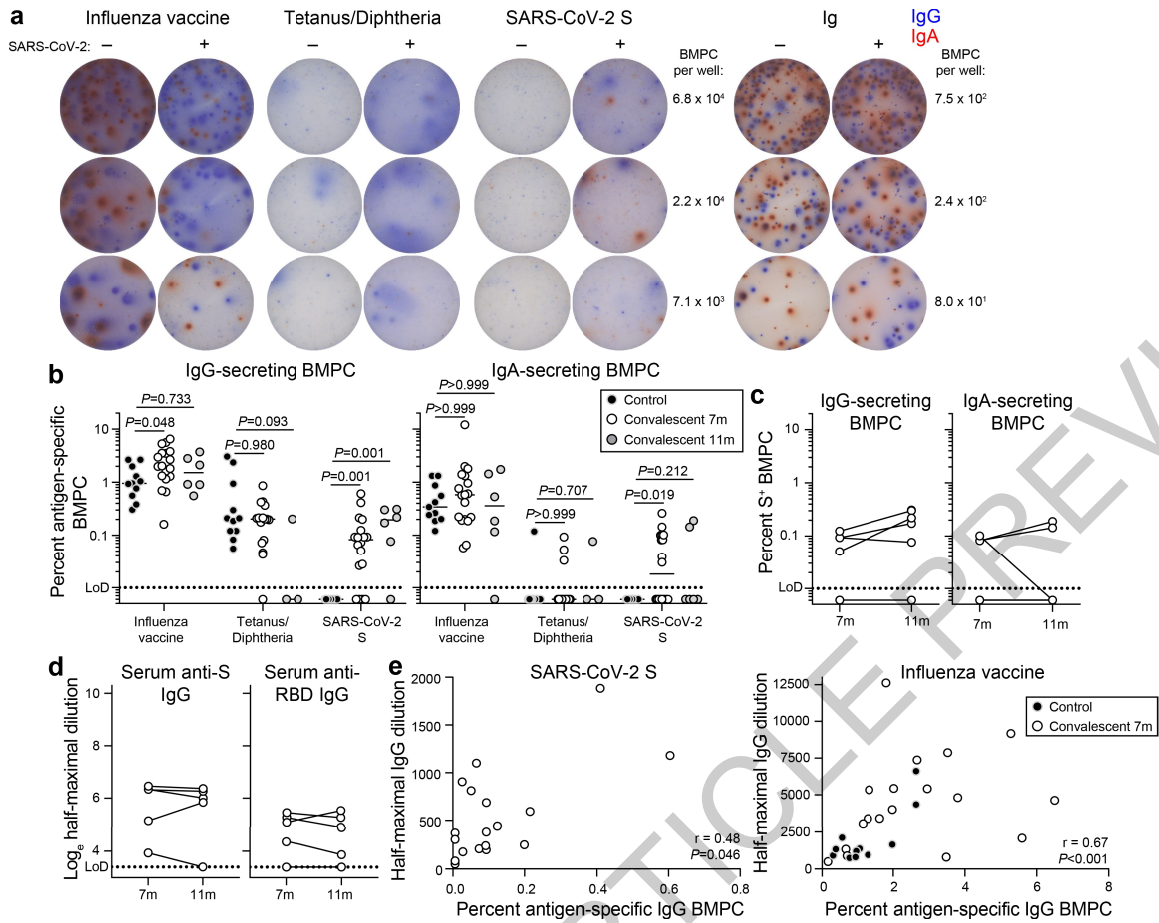


**Fig. 2 | SARS-CoV-2 infection elicits S-binding long-lived BMPCs.**

**a**, Representative images of ELISpot wells coated with the indicated antigens or anti-Ig and developed in blue and red for IgG and IgA, respectively after incubation of magnetically enriched BMPC from convalescent and control participants. **b**, Frequencies of BMPC secreting IgG (*left*) or IgA (*right*) antibodies specific for the indicated antigens, indicated as percentages of total IgG- or IgA-secreting BMPC in control (black circles) or convalescent participants 7m (white circles) or 11m (grey circles) post symptom onset. Horizontal lines indicate medians. *P*-values from two-sided Kruskal-Wallis tests with Dunn's correction for multiple comparisons between control and convalescent participants. Each symbol represents one sample

(*n*=18 convalescent, 11 control). **c**, Paired frequencies of BMPC secreting IgG (*left*) and IgA (*right*) specific for S from convalescent participants 7m and 11m post symptom onset. **d**, Paired anti-S (*left*) and anti-RBD (*right*) IgG serum antibody titers from convalescent participants 7m and 11m post symptom onset. Data in panels (c) and (d, *left*) are also shown in (b) and Fig. 1b, respectively. Each symbol represents one sample (*n*=5). **e**, Frequencies of IgG BMPC specific for S (*left*) and influenza virus vaccine (*right*) plotted against respective IgG titers in paired blood samples from control (black circles) or convalescent participants 7m post symptom onset (white circles). *P*- and *r*-values from two-sided Spearman's correlations. Each symbol represents one sample (*n*=18 convalescent, 11 control).

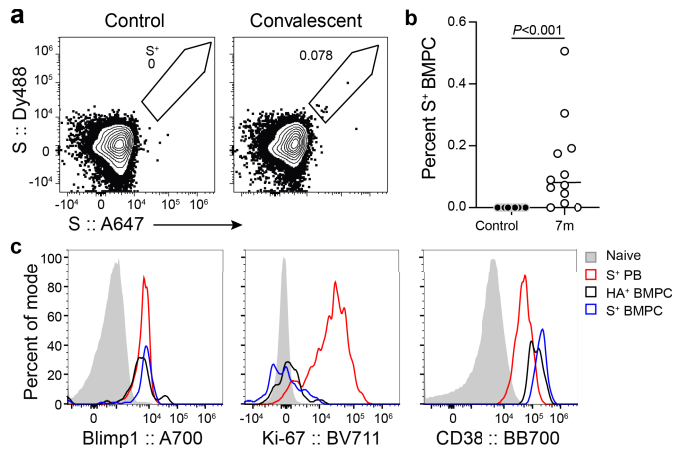


**Fig. 3 | SARS-CoV-2 BMPCs are quiescent and distinct from circulating PBs.**  
**a**, Representative plots of intracellular S staining in CD20<sup>lo</sup> CD38<sup>+</sup> IgD<sup>lo</sup> CD19<sup>hi/lo</sup> CD3<sup>-</sup> live singlet BMPCs (gating in Extended Data Fig. 1a) from control (*left*) and convalescent (*right*) magnetically enriched BMPC 7 months after symptom onset. **b**, Frequencies of S-binding BMPCs in total BMPC from control (black circles) or convalescent participants 7m post symptom onset (white circles). Horizontal lines indicate medians. *P*-value from two-sided Mann-Whitney U-test. Each symbol represents one sample (*n*=12 convalescent, 9 control). **c**, Histograms of Blimp1 (*left*), Ki-67 (*center*), and CD38 (*right*) staining on S<sup>+</sup> (blue) and HA<sup>+</sup> (black) BMPC from magnetically enriched BMPC 7m post symptom onset and S<sup>+</sup> plasmablasts (red), and naive B cells (grey) from healthy donor PBMC 1 week after SARS-CoV-2 S immunization.

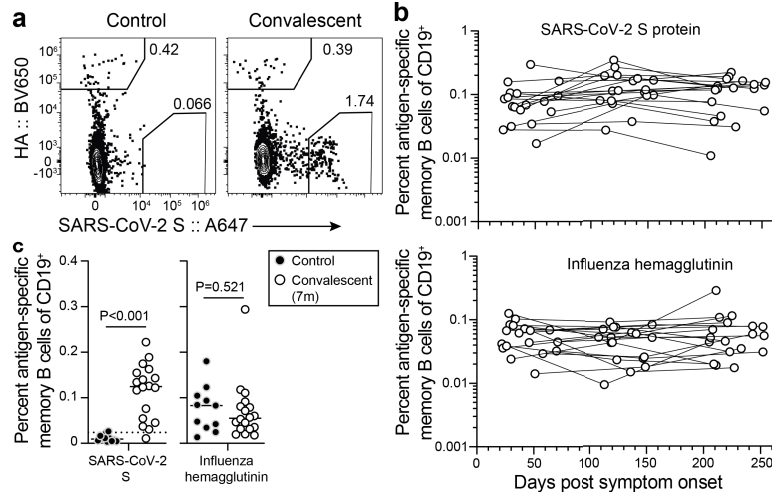


**Fig. 4 | SARS-CoV-2 infection elicits a robust memory B cell response.**

**a**, Representative plots of surface influenza virus hemagglutinin (HA) and S staining on CD20<sup>+</sup> CD38<sup>lo/int</sup> IgD<sup>lo</sup> CD19<sup>+</sup> CD3<sup>-</sup> live singlet memory B cells (gating in Extended Data Fig. 1d) from control (*left*) and convalescent (*right*) PBMCs 7 months after symptom onset. **b**, Kinetics of S- (*top*) and HA- (*bottom*) binding memory B cells in PBMCs from convalescent patients collected at the indicated days post onset of symptoms. Data from the 7-month timepoint are also shown

in (c). **c**, Frequencies of S- (*left*) and HA- (*right*) binding memory B cells in PBMC from control (black circles) and convalescent (white circles) participants 7 months after symptom onset. The dotted line in the S plot indicates limit of sensitivity, defined as the median + 2× SD of the controls. Each symbol represents one sample ( $n=18$  convalescent, 11 control). Horizontal lines indicate medians.  $P$ -values from two-sided Mann-Whitney U-tests.

### Sample collection, preparation, and storage

All studies were approved by the Institutional Review Board of Washington University in St. Louis. Written consent was obtained from all participants. Seventy-seven participants who had recovered from SARS-CoV-2 infection and eleven controls without SARS-CoV-2 infection history were enrolled (Extended Data Tables 1 and 3). Blood samples were collected in EDTA tubes and peripheral blood mononuclear cells (PBMCs) were enriched by density gradient centrifugation over Ficoll 1077 (GE) or Lymphopure (BioLegend), remaining red blood cells were lysed with ammonium chloride lysis buffer, and cells were immediately used or cryopreserved in 10% dimethylsulfoxide in FBS. Approximately 30 mL bone marrow aspirates were collected in EDTA tubes from the iliac crest of eighteen convalescent participants and the controls. Bone marrow mononuclear cells were enriched by density gradient centrifugation over Ficoll 1077, remaining red blood cells were lysed with ammonium chloride buffer (Lonza) and washed with PBS supplemented with 2% FBS and 2 mM EDTA. Bone marrow plasma cells were enriched from bone marrow mononuclear cells using CD138 Positive Selection Kit II (Stemcell) and immediately used for ELISpot or cryopreserved in 10% dimethylsulfoxide in FBS for flow cytometric analysis.

### Antigens

Recombinant soluble spike protein (S) and its receptor binding domain (RBD) derived from SARS-CoV-2 was expressed as previously described<sup>35</sup>. Briefly, mammalian cell codon-optimized nucleotide sequences coding for the soluble version of S (GenBank: MN908947.3, amino acids 1-1213) including a C-terminal thrombin cleavage site, T4 foldon trimerization domain, and hexahistidine tag cloned into mammalian expression vector pCAGGS. The S protein sequence was modified to remove the polybasic cleavage site (RRAR to A) and two stabilizing mutations were introduced (K986P and V987P, wild type numbering). RBD, along with the signal peptide (amino acids 1-14) plus a hexahistidine tag were cloned into mammalian expression vector pCAGGS. Recombinant proteins were produced in Expi293F cells (ThermoFisher) by transfection with purified DNA using the ExpiFectamine 293 Transfection Kit (ThermoFisher). Supernatants from transfected cells were harvested 3 (for S) or 4 (for RBD) days post-transfection, and recombinant proteins were purified using Ni-NTA agarose (ThermoFisher), then buffer exchanged into phosphate buffered saline (PBS) and concentrated using Amicon Ultra-cel centrifugal filters (EMD Millipore). For flow cytometry staining, recombinant S was labeled with Alexa Fluor 647- or DyLight 488-NHS ester (Thermo Fisher); excess Alexa Fluor 647 and DyLight 488 were removed using 7-kDa and 40-kDa Zeba desalting columns, respectively (Pierce). Recombinant HA from A/Michigan/45/2015 (a.a. 18-529, Immune Technology) was labeled with DyLight 405-NHS ester (Thermo Fisher); excess DyLight 405 was removed using 7-kDa Zeba desalting columns. Recombinant HA from A/Brisbane/02/2018 (a.a. 18-529) and B/Colorado/06/2017 (a.a. 18-546) (both Immune Technology) were biotinylated using the EZ-Link Micro NHS-PEG4-Biotinylation Kit (Thermo Fisher); excess biotin was removed using 7-kDa Zeba desalting columns.

### ELISpot

Plates were coated with Flucelvax Quadrivalent 2019/2020 seasonal influenza virus vaccine (Sequiris), tetanus/diphtheria vaccine (Grifols), recombinant S, or anti-human Ig. Direct *ex-vivo* ELISpot was performed to determine the number of total, vaccine-binding, or recombinant S-binding IgG- and IgA-secreting cells present in BMPC and PBMC samples using IgG/IgA double-color ELISpot Kits (Cellular Technologies, Ltd.) according to the manufacturer's instructions. ELISpot plates were analyzed using an ELISpot counter (Cellular Technologies Ltd.).

### ELISA

Assays were performed in 96-well plates (MaxiSorp; Thermo) coated with 100  $\mu$ L of Flucelvax 2019/2020 or recombinant S in PBS, and plates were incubated at 4  $^{\circ}$ C overnight. Plates were then blocked with 10% FBS and 0.05% Tween20 in PBS. Serum or plasma were serially diluted in blocking buffer and added to the plates. Plates were incubated for 90 min at room temperature and then washed 3 times with 0.05% Tween-20 in PBS. Goat anti-human IgG-HRP (Jackson ImmunoResearch, 1:2,500) was diluted in blocking buffer before adding to wells and incubating for 60 min at room temperature. Plates were washed 3 times with 0.05% Tween20 in PBS, and then washed 3 times with PBS before the addition of o-Phenylenediamine dihydrochloride peroxidase substrate (Sigma-Aldrich). Reactions were stopped by the addition of 1 M HCl. Optical density measurements were taken at 490 nm. The half-maximal binding dilution for each serum or plasma sample was calculated using nonlinear regression (Graphpad Prism v8). The limit of detection was defined as 1:30.

### Statistics

Spearman's correlation coefficients were estimated to assess the relationship between 7-month anti-S and anti-influenza virus vaccine IgG titers and frequencies of BMPCs secreting IgG specific for S and influenza virus vaccine, respectively. Means and pairwise differences of antibody titers at each timepoint were estimated using a linear mixed model analysis with a first order autoregressive covariance structure. Time since symptom onset was treated as a categorical fixed effect for the four different sample time points spaced approximately 3 months apart. *P*-values were adjusted for multiple comparisons using Tukey's method. All analyses were conducted using SAS 9.4 (SAS Institute Inc, Cary, NC, USA) and Prism 8.4 (Graphpad), and *P*-values < 0.05 were considered significant.

### Flow cytometry

Staining for flow cytometry analysis was performed using cryo-preserved magnetically enriched BMPC and cryo-preserved PBMC. For BMPC staining, cells were stained for 30 min on ice with CD45-A532 (HI30, Thermo, 1:50), CD38-BB700 (HIT2, BD Horizon, 1:500), CD19-PE (HIB19, 1:200), CXCR5-PE-Dazzle 594 (J252D4, 1:50), CD71-PE-Cy7 (CY1G4, 1:400), CD20-APC-Fire750 (2H7, 1:400), CD3-APC-Fire810 (SK7, 1:50), and Zombie Aqua (all BioLegend) diluted in Brilliant Staining buffer (BD Horizon). Cells were washed twice with 2% FBS and 2 mM EDTA in PBS (P2), fixed for 1h using the TrueNuclear permeabilization kit (BioLegend), washed twice with perm/wash buffer, stained for 1h with DyLight 405-conjugated recombinant HA from A/Michigan/45/2015, DyLight 488- and Alexa 647-conjugated S, Ki-67-BV711 (Ki-67, 1:200, BioLegend), and Blimp1-A700 (646702, 1:50, R&D), washed twice with perm/wash buffer, and resuspended in P2. For memory B cell staining, PBMC were stained for 30 min on ice with biotinylated recombinant HAs diluted in P2, washed twice, then stained for 30 min on ice with Alexa 647-conjugated S, IgA-FITC (M24A, Millipore, 1:500), IgG-BV480 (goat polyclonal, Jackson ImmunoResearch, 1:100), IgD-SB702 (IA6-2, Thermo, 1:50), CD38-BB700 (HIT2, BD Horizon, 1:500), CD20-Pacific Blue (2H7, 1:400), CD4-BV570 (OKT4, 1:50), CD24-BV605 (ML5, 1:100), streptavidin-BV650, CD19-BV750 (HIB19, 1:100), CD71-PE (CY1G4, 1:400), CXCR5-PE-Dazzle 594 (J252D4, 1:50), CD27-PE-Cy7 (O323, 1:200), IgM-APC-Fire750 (MHM-88, 1:100), CD3-APC-Fire810 (SK7, 1:500), and Zombie NIR (all BioLegend) diluted in Brilliant Staining buffer (BD Horizon), and washed twice with P2. Cells were acquired on an Aurora using SpectroFlo v2.2 (Cytek). Flow cytometry data were analyzed using FlowJo v10 (Treestar). In each experiment, PBMC were included from convalescent and control participants.

### Reporting summary

Further information on research design is available in the Nature Research Reporting Summary linked to this paper.

## Data availability statement

Relevant data are available from the corresponding author upon reasonable request.

35. Stadlbauer, D. *et al.* SARS-CoV-2 Seroconversion in Humans: A Detailed Protocol for a Serological Assay, Antigen Production, and Test Setup. *Curr. Protoc. Microbiol.* **57**, (2020).

**Acknowledgements** We thank the generous participation of the donors for providing precious specimens. We thank Lisa Kessels, AJ Winingham, the staff of the Infectious Diseases Clinical Research Unit at Washington University School of Medicine, and the nursing team of the bone marrow biopsy suite at Washington University School of Medicine and Barnes Jewish Hospital for sample collection and providing care for donors. The SARS-CoV-2 S and RBD protein expression plasmids were kindly provided by F. Krammer (Icahn School of Medicine at Mt Sinai). The Ellebedy laboratory was supported by National Institute of Allergy and Infectious Diseases (NIAID) grants U01AI141990 and 1U01AI150747, NIAID Centers of Excellence for Influenza Research and Surveillance contracts HHSN272201400006C and HHSN272201400008C, and NIAID Collaborative Influenza Vaccine Innovation Centers contract 75N93019C00051. J.S.T. was supported by NIAID 5T32CA009547. L.H. was supported by Norwegian Research Council grant 271160 and National Graduate School in Infection Biology and Antimicrobials grant 249062. This study utilized samples obtained from the Washington University School of Medicine's COVID-19 biorepository supported by the NIH/ National Center for Advancing Translational Sciences grant UL1 TR002345. The content is solely the responsibility of the authors and does not necessarily represent the view of the NIH.

The WU353, WU367, and 368 studies were reviewed and approved by the Washington University Institutional Review Board (approval nos. 202003186, 202009100, and 202012081, respectively).

**Author contributions** A.H.E. conceived and designed the study. J.S.T. and A.H.E. designed experiments and composed the manuscript., A.H., M.K.K., I.P., J.A.O., and R.M.P. wrote and maintained the IRB protocol, recruited, and phlebotomized participants and coordinated sample collection. J.S.T., W.K., E.K., A.J.S., and L.H. processed specimens. A.J.S. expressed S and RBD proteins. J.S.T., W.K., and E.K. performed ELISA and ELISpot. J.S.T. performed flow cytometry. J.S.T., A.M.R., C.W.G. and A.H.E. analyzed data. All authors reviewed the manuscript.

**Competing interests** The Ellebedy laboratory received funding under sponsored research agreements that are unrelated to the data presented in the current study from Emergent BioSolutions and from AbbVie. J.S.T., A.J.S., and A.H.E. are recipients of a licensing agreement with Abbvie Inc. unrelated to the data presented in the current study. A.H.E. is a consultant for Mubadala Investment Company and the founder of ImmuneBio Consulting LLC. All other authors declare no competing interests.

### Additional information

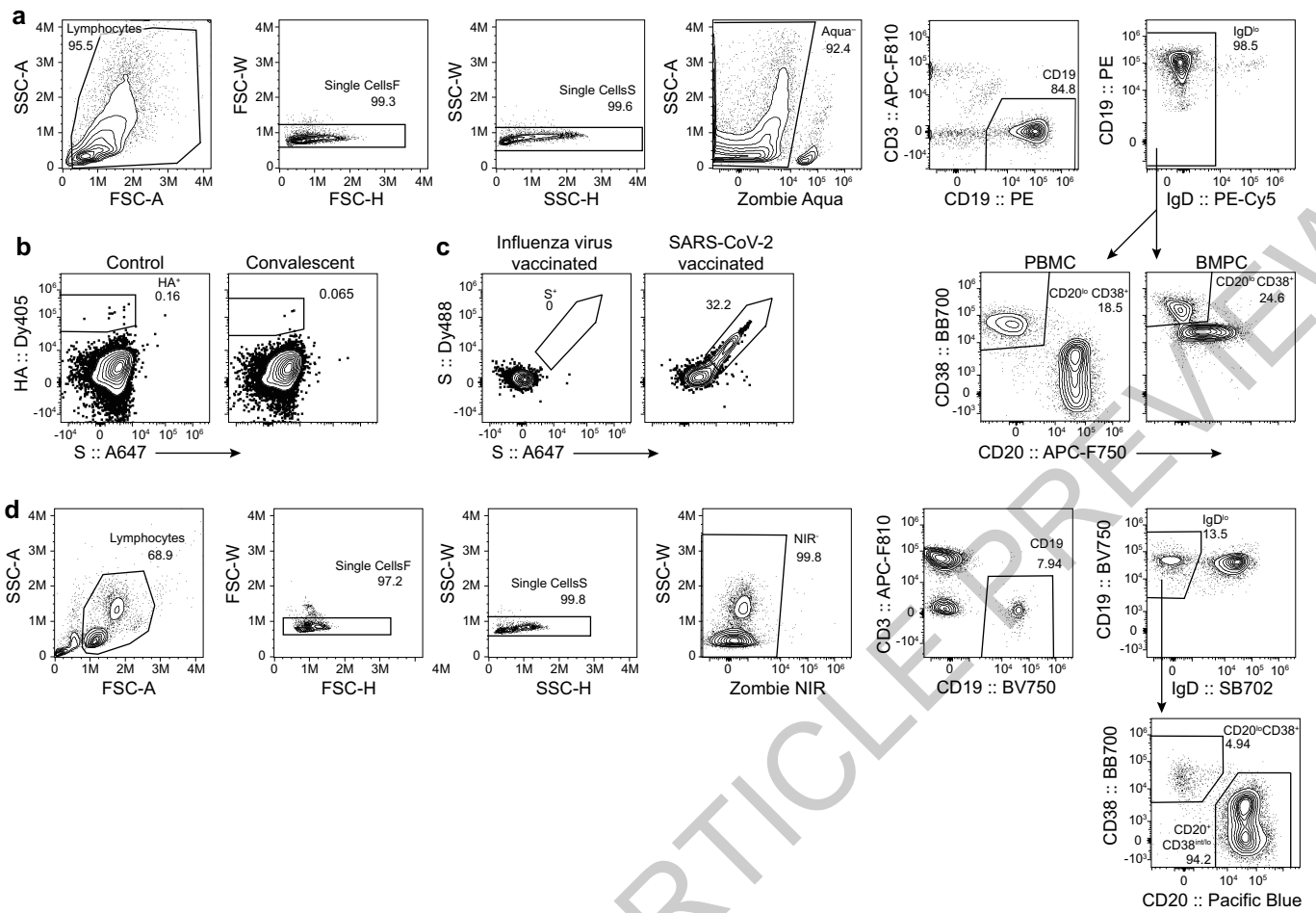
**Supplementary information** The online version contains supplementary material available at <https://doi.org/10.1038/s41586-021-03647-4>.

**Correspondence and requests for materials** should be addressed to A.H.E.

**Peer review information** *Nature* thanks Stanley Perlman, Andreas Radbruch and the other, anonymous, reviewer(s) for their contribution to the peer review of this work. Peer reviewer reports are available.

**Reprints and permissions information** is available at <http://www.nature.com/reprints>.

ACCELERATED ARTICLE PREVIEW



**Extended Data Fig. 1 | Flow cytometry identification of SARS-CoV-2 elicited plasma cells and memory B cells. a, d,** Flow cytometry gating strategies for BMPC in magnetically enriched BMPC and plasmablasts in PBMC (a) and isotype-switched memory B cells and plasmablasts in PBMC (d). **b,** Representative plots of intracellular S and influenza virus hemagglutinin

(HA) staining in BMPC from control (*left*) and convalescent (*right*) samples 7 months after symptom onset. **c,** Representative plots of intracellular S staining in plasmablasts in PBMC 1 week after seasonal influenza virus or SARS-CoV-2 vaccination.

Extended Data Table 1 | SARS-CoV-2 convalescent patient demographics

	Total N=77 N (%)	Bone marrow biopsy N=19 N (%)
<b>Age (median [range])</b>	49 (21-69)	52 (30-69)
<b>Sex</b>		
Female	38 (49.4)	7 (36.8)
Male	39 (50.6)	12 (63.2)
<b>Race</b>		
White	70 (90.9)	18 (94.7)
Black	1 (1.3)	0 (0)
Asian	4 (5.2)	0 (0)
Other	2 (2.6)	1 (5.3)
<b>Comorbidities</b>		
Asthma	13 (16.9)	3 (15.8)
Lung disease	0 (0)	0 (0)
Heart disease	3 (3.9)	0 (0)
Hypertension	13 (16.9)	6 (31.6)
Diabetes mellitus	3 (3.9)	3 (15.8)
Cancer	10 (13)	3 (15.8)
Autoimmune disease	4 (5.2)	2 (10.5)
Hyperlipidemia	8 (10.4)	2 (10.5)
Hypothyroidism	5 (6.5)	3 (15.8)
Gastroesophageal reflux disease	5 (6.5)	2 (10.5)
Other	26 (33.8)	10 (52.6)
<i>Solid organ transplant</i>	1 (1.3)	1 (5.3)
<i>Obesity</i>	1 (1.3)	0 (0)

ACCELERATED ARTICLE PREVIEW

Extended Data Table 2 | SARS-CoV-2 convalescent patient symptoms

	Total N=77 N (%)	Bone marrow biopsy N=19 N (%)
<b>First symptom</b>		
Cough	12 (15.6)	3 (15.8)
Diarrhea	1 (1.3)	0 (0)
Dyspnea	2 (2.6)	1 (5.3)
Fatigue	7 (9.1)	0 (0)
Fever	22 (28.6)	9 (47.4)
Headache	8 (10.4)	2 (10.5)
Loss of taste	3 (3.9)	2 (10.5)
Malaise	4 (5.2)	1 (5.3)
Myalgias	9 (11.7)	0 (0)
Nasal congestion	2 (2.6)	0 (0)
Nausea	1 (1.3)	0 (0)
Night sweats	1 (1.3)	0 (0)
Sore throat	5 (6.5)	1 (5.3)
<b>Symptom present during disease</b>		
Fever	65 (84.4)	17 (89.5)
Cough	54 (70.1)	14 (73.7)
Dyspnea	31 (40.3)	11 (57.9)
Nausea	19 (24.7)	4 (21.1)
Vomiting	9 (11.7)	3 (15.8)
Diarrhea	39 (50.6)	10 (52.6)
Headaches	47 (61)	12 (63.2)
Loss of taste	42 (54.5)	11 (57.9)
Loss of smell	42 (54.5)	10 (52.6)
Fatigue	38 (49.4)	7 (36.8)
Malaise	6 (7.8)	1 (5.3)
Myalgias or body aches	34 (44.2)	8 (42.1)
Sore throat	12 (15.6)	1 (5.3)
Chills	25 (32.5)	6 (31.6)
Nasal congestion	6 (7.8)	0 (0)
Other	32 (41.6)	7 (36.8)
<b>Duration of symptoms in days (median [range])</b>	14 (1-43)	13 (6-30)
<b>Days from symptom onset to positive SARS-CoV-2 PCR test (median [range])</b>	6 (0-36)	6 (1-31)
<b>Days from symptom onset to 1-month blood sample collection (median [range])</b>	41 (21-84)	34 (22-71)
<b>Hospitalization</b>	6 (7.8)	1 (5.3)
<b>COVID medications</b>		
Hydroxychloroquine	2 (2.6)	0 (0)
Chloroquine	1 (1.3)	0 (0)
Azithromycin	14 (18.2)	6 (31.6)
Lopinavir/ritonavir	0 (0)	0 (0)
Remdesivir	0 (0)	0 (0)
Convalescent plasma	0 (0)	0 (0)
None	61 (79.2)	12 (63.2)
Other	2 (2.6)	1 (5.3)

**Extended Data Table 3 | SARS-CoV-2 convalescent patient symptoms and follow up samples (months 4–11)**

	Month 4		Month 7		Month 11	
	Total N= 76 N (%)	Bone marrow biopsy N=19 N (%)	Total N= 76 N (%)	Bone marrow biopsy N=18 N (%)	Total N= 42 N (%)	Bone marrow biopsy N=12 N (%)
<b>Days from positive SARS-CoV-2 PCR test to follow up visit (median [range])</b>	125 (102-192)	117 (105-150)	222 (191-275)	213 (200-247)	308 (283-369)	303 (283-325)
<b>Days from symptom onset to blood sample collection (median [range])</b>	131 (106-193)	124 (108-155)	227 (194-277)	222 (205-253)	314 (288-373)	309 (297-343)
<b>Any symptom present at follow up visit</b>	25 (32.9)	8 (42.1)	33 (43)	10 (55.6)	20 (47.6)	6 (50)
Fever	0 (0)	0 (0)	2 (2.6)	0 (0)	1 (2.4)	0 (0)
Cough	1 (1.3)	1 (5.3)	0 (0)	0 (0)	1 (2.4)	0 (0)
Dyspnea	7 (9.2)	2 (10.5)	6 (7.9)	3 (16.7)	6 (14.3)	3 (25)
Nausea	1 (1.3)	0 (0)	1 (1.3)	0 (0)	0 (0)	0 (0)
Vomiting	1 (1.3)	1 (5.3)	0 (0)	0 (0)	0 (0)	0 (0)
Diarrhea	2 (2.6)	1 (5.3)	1 (1.3)	0 (0)	0 (0)	0 (0)
Headaches	1 (1.3)	0 (0)	3 (3.9)	0 (0)	2 (4.8)	0 (0)
Loss or altered taste	8 (10.5)	0 (0)	9 (11.8)	1 (5.6)	5 (11.9)	1 (8.3)
Loss or altered smell	13 (17.1)	2 (10.5)	12 (15.8)	2 (11.1)	8 (19)	2 (16.7)
Fatigue	9 (11.8)	4 (21.1)	13 (17.1)	5 (27.8)	8 (19)	3 (25)
Forgetfulness/brain fog	8 (10.5)	6 (31.6)	12 (15.8)	6 (33.3)	10 (23.8)	4 (33.3)
Hair loss	5 (6.6)	1 (5.3)	3 (3.9)	1 (5.6)	2 (4.8)	0 (0)
Other	7 (9.2)	3 (15.8)	12 (15.8)	1 (5.6)	10 (23.8)	1 (8.3)
<i>Joint pain</i>	3 (3.9)	1 (5.3)	7 (9.2)	1 (5.3)	3 (7.1)	0 (0)

ACCELERATED ARTICLE PREVIEW

# Article

Extended Data Table 4 | Healthy control demographics

Variable	Total N= 11 N (%)
Age (median [range])	38 (23-53)
<b>Sex</b>	
Female	4 (36.4)
Male	7 (63.6)
<b>Race</b>	
White	8 (72.7)
Black	1 (9.1)
Asian	1 (9.1)

ACCELERATED ARTICLE PREVIEW

## Reporting Summary

Nature Research wishes to improve the reproducibility of the work that we publish. This form provides structure for consistency and transparency in reporting. For further information on Nature Research policies, see [Authors & Referees](#) and the [Editorial Policy Checklist](#).

### Statistics

For all statistical analyses, confirm that the following items are present in the figure legend, table legend, main text, or Methods section.

n/a Confirmed

- The exact sample size ( $n$ ) for each experimental group/condition, given as a discrete number and unit of measurement
- A statement on whether measurements were taken from distinct samples or whether the same sample was measured repeatedly
- The statistical test(s) used AND whether they are one- or two-sided  
*Only common tests should be described solely by name; describe more complex techniques in the Methods section.*
- A description of all covariates tested
- A description of any assumptions or corrections, such as tests of normality and adjustment for multiple comparisons
- A full description of the statistical parameters including central tendency (e.g. means) or other basic estimates (e.g. regression coefficient) AND variation (e.g. standard deviation) or associated estimates of uncertainty (e.g. confidence intervals)
- For null hypothesis testing, the test statistic (e.g.  $F$ ,  $t$ ,  $r$ ) with confidence intervals, effect sizes, degrees of freedom and  $P$  value noted  
*Give  $P$  values as exact values whenever suitable.*
- For Bayesian analysis, information on the choice of priors and Markov chain Monte Carlo settings
- For hierarchical and complex designs, identification of the appropriate level for tests and full reporting of outcomes
- Estimates of effect sizes (e.g. Cohen's  $d$ , Pearson's  $r$ ), indicating how they were calculated

*Our web collection on [statistics for biologists](#) contains articles on many of the points above.*

### Software and code

Policy information about [availability of computer code](#)

Data collection Flow cytometry data were acquired using SpectroFlo software v2.2.

Data analysis Flow cytometry data were analyzed using FlowJo v10 and Prism v8  
ELISA and ELISpot data were analyzed using Prism v8 and SAS 9.4

For manuscripts utilizing custom algorithms or software that are central to the research but not yet described in published literature, software must be made available to editors/reviewers. We strongly encourage code deposition in a community repository (e.g. GitHub). See the Nature Research [guidelines for submitting code & software](#) for further information.

### Data

Policy information about [availability of data](#)

All manuscripts must include a [data availability statement](#). This statement should provide the following information, where applicable:

- Accession codes, unique identifiers, or web links for publicly available datasets
- A list of figures that have associated raw data
- A description of any restrictions on data availability

All relevant data are available from the corresponding author upon reasonable request.

### Field-specific reporting

Please select the one below that is the best fit for your research. If you are not sure, read the appropriate sections before making your selection.

- Life sciences       Behavioural & social sciences       Ecological, evolutionary & environmental sciences

## Life sciences study design

All studies must disclose on these points even when the disclosure is negative.

Sample size	No statistical methods were used to determine sample size. 77 convalescent patients and 11 control participants were enrolled based on recruitment; these numbers provided sufficient power to determine differences in SARS-CoV-2 responses between the groups.
Data exclusions	No data were excluded
Replication	Samples were collected from 77 convalescent patients and 11 control participants. ELISA for each participant at each timepoint was performed once with two technical replicates. ELISpot and flow cytometry experiments were performed once for each sample at each timepoint.
Randomization	Different experimental groups were not assigned.
Blinding	No blinding was done in this study; subjective measurements were not made.

## Reporting for specific materials, systems and methods

We require information from authors about some types of materials, experimental systems and methods used in many studies. Here, indicate whether each material, system or method listed is relevant to your study. If you are not sure if a list item applies to your research, read the appropriate section before selecting a response.

### Materials & experimental systems

n/a	Involved in the study
<input type="checkbox"/>	<input checked="" type="checkbox"/> Antibodies
<input type="checkbox"/>	<input checked="" type="checkbox"/> Eukaryotic cell lines
<input checked="" type="checkbox"/>	<input type="checkbox"/> Palaeontology
<input checked="" type="checkbox"/>	<input type="checkbox"/> Animals and other organisms
<input type="checkbox"/>	<input checked="" type="checkbox"/> Human research participants
<input checked="" type="checkbox"/>	<input type="checkbox"/> Clinical data

### Methods

n/a	Involved in the study
<input checked="" type="checkbox"/>	<input type="checkbox"/> ChIP-seq
<input type="checkbox"/>	<input checked="" type="checkbox"/> Flow cytometry
<input checked="" type="checkbox"/>	<input type="checkbox"/> MRI-based neuroimaging

## Antibodies

Antibodies used	IgG-HRP (goat polyclonal, Jackson ImmunoResearch 109-035-088), IgG-BV480 (goat polyclonal, Jackson ImmunoResearch 109-685-098), IgD-SB702 (IA6-2, Thermo 67-9868-42), IgA-FITC (M24A, Millipore CBL114F), CD45-A532 (HI30, Thermo 58-0459-42), CD38-BB700 (HIT2, BD Horizon 566445), Blimp1-A700 (646702, R&D IC36081N), CD20-Pacific Blue (2H7, 302320), CD4-BV570 (OKT4, 317445), CD24-BV605 (ML5, 311124), streptavidin-BV650 (405232), Ki-67-BV711 (Ki-67, 350516), CD19-BV750 (HIB19, 302262), CD19-PE (HIB19, 302254), CD71-PE (CY1G4, 334106), CXCR5-PE-Dazzle 594 (J252D4, 356928), CD27-PE-Cy7 (O323, 302838), CD71-PE-Cy7 (CY1G4, 334112), CD20-APC-Fire750 (2H7, 302358), IgM-APC-Fire750 (MHM-88, 314546), CD3-APC-Fire810 (SK7, 344858); all Biolegend.
Validation	Commercial antibodies were validated by their respective manufacturers per their associated data sheets and titrated in the lab for their respective assay (ELISA or flow cytometry) by serial dilution

## Eukaryotic cell lines

Policy information about [cell lines](#)

Cell line source(s)	Expi293F (Thermo)
Authentication	The cell line was not authenticated
Mycoplasma contamination	Cell lines were not tested for mycoplasma contamination. Growth rates were consistent with manufacturer's published data.
Commonly misidentified lines (See <a href="#">ICLAC</a> register)	No commonly misidentified cell lines were used

## Human research participants

Policy information about [studies involving human research participants](#)

Population characteristics	77 SARS-CoV-2 convalescent study participants were recruited, ages 21-69, 49.4% female, 50.6% male 11 healthy control participants with no history of SARS-CoV-2 infection were recruited, ages 23-53, 36.4% female, 63.6% male
Recruitment	Study participants were recruited from the St. Louis metropolitan area by the Washington University Clinical Trials Unit. Potential self-selection and recruiting biases are unlikely to affect the parameters we measured.
Ethics oversight	The study was approved by the Washington University IRB

Note that full information on the approval of the study protocol must also be provided in the manuscript.

## Flow Cytometry

### Plots

Confirm that:

- The axis labels state the marker and fluorochrome used (e.g. CD4-FITC).
- The axis scales are clearly visible. Include numbers along axes only for bottom left plot of group (a 'group' is an analysis of identical markers).
- All plots are contour plots with outliers or pseudocolor plots.
- A numerical value for number of cells or percentage (with statistics) is provided.

### Methodology

Sample preparation	Peripheral blood and bone marrow mononuclear cells were isolated from EDTA anticoagulated blood and bone marrow aspirates, respectively using density gradient centrifugation, and remaining RBCs were lysed with ammonium chloride lysis buffer. Bone marrow plasma cells were magnetically enriched from bone marrow mononuclear cells and immediately used for ELISpot or cryopreserved in 10% dimethylsulfoxide in FBS for flow cytometric analysis. PBMCs were immediately used or cryopreserved in 10% DMSO in FBS.
Instrument	Cytek Aurora
Software	Flow cytometry data were acquired using Cytek SpectroFlo software, and analyzed using FlowJo (Treestar) v10.
Cell population abundance	Cells were not sorted
Gating strategy	Gating strategies are shown in extended data figure

- Tick this box to confirm that a figure exemplifying the gating strategy is provided in the Supplementary Information.